Article

Structure

Homer Tetramer Promotes Actin Bundling Activity of Drebrin

Graphical Abstract

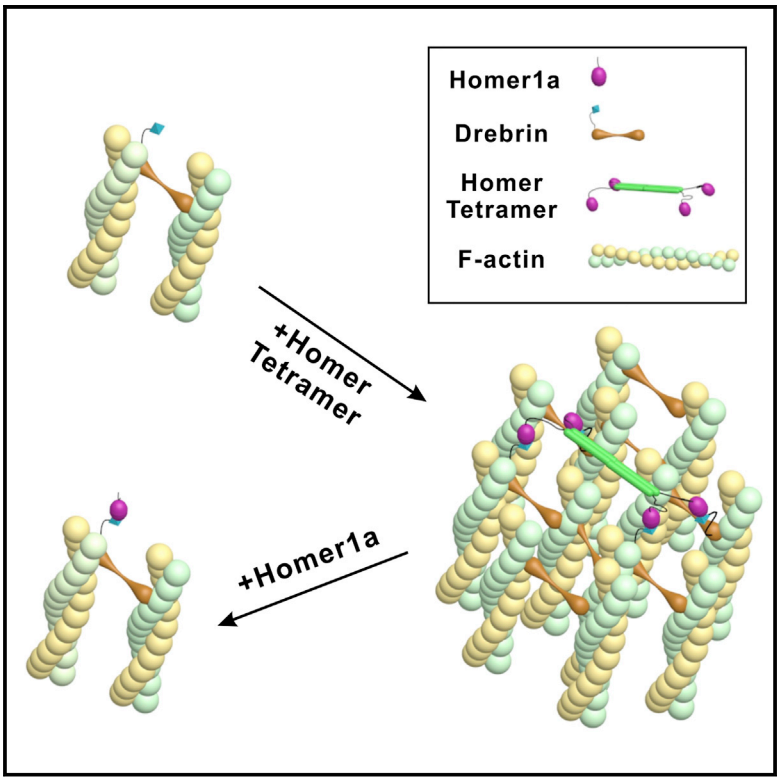

Authors

Zhiwei Li, Haiyang Liu, Jianchao Li, ..., Jun Wan, Wei Liu, Mingjie Zhang

Correspondence

liuwei@sphmc.org (W.L.), mzhang@ust.hk (M.Z.)

In Brief

The crystal structure of Drebrin-HBM1/Homer-EVH1 reveals an extended Homer EVH1 binding motif. Homer tetramer promotes actin bundling activity of Drebrin and stimulates Drebrin-induced filopodia formation in cells, suggesting a potential role of Homer1 in modulating synaptic spine homeostatic scaling via binding to Drebrin.

Highlights

- Homer EVH1 specifically binds to the first Homer binding motif of Drebrin
- Homer-EVH1/Drebrin-HBM1 structure reveals an extended EVH1 binding motif
- Homer tetramer promotes actin bundling activity of Drebrin
- Homer1a antagonizes Homer1b in Drebrin-stimulated actin bundling

Data Resources

5ZZ9

Li et al., 2019, Structure *27*, 27–38
January 2, 2019
https://doi.org/10.1016/j.str.2018.10.011

CellPress

Structure
Article

Homer Tetramer Promotes Actin Bundling Activity of Drebrin

Zhiwei Li,[1,4] Haiyang Liu,[1,2,4] Jianchao Li,[2] Qingqing Yang,[1] Zhe Feng,[2] Yujie Li,[3] Haibin Yang,[3] Cong Yu,[3] Jun Wan,[1,2] Wei Liu,[1,*] and Mingjie Zhang[1,2,5,*]

[1]Shenzhen Key Laboratory for Neuronal Structural Biology, Biomedical Research Institute, Shenzhen Peking University-The Hong Kong University of Science and Technology Medical Center, Shenzhen 518036, China

[2]Division of Life Science, State Key Laboratory of Molecular Neuroscience, Hong Kong University of Science and Technology, Clear Water Bay, Kowloon, Hong Kong, China

[3]Department of Biology, Southern University of Science and Technology, Shenzhen 518055, China

[4]These authors contributed equally

[5]Lead Contact

*Correspondence: liuwei@sphmc.org (W.L.), mzhang@ust.hk (M.Z.)

https://doi.org/10.1016/j.str.2018.10.011

SUMMARY

Drebrin is an actin bundling protein that plays critical roles in synaptic spine development and plasticity. Homer, one of the most abundant scaffolding proteins in postsynaptic density, interacts with Drebrin's C-terminal PPXXF motifs using its Ena/VASP homology 1 (EVH1) domain. However, the molecular mechanism and biological function of this interaction remain unclear. Here we show that Homer specifically binds to the first but not the second PPXXF motif in Drebrin. The crystal structure of Drebrin-Homer binding motif 1 in complex with Homer EVH1 reveals a consensus Homer EVH1 binding motif. Homer tetramer promotes actin bundling activity of Drebrin *in vitro* and stimulates Drebrin-induced filopodia formation and elongation in cells. We further show that monomeric Homer1a antagonizes Homer1b in promoting Drebrin-stimulated actin bundling. Our study suggests a potential regulatory role of Homer1 in modulating excitatory synaptic spine homeostatic scaling via binding to Drebrin.

INTRODUCTION

Drebrin (developmentally regulated brain protein), originally identified in neurons (Shirao and Obata, 1985), contains two major isoforms, A and E (Kojima et al., 1993; Shirao et al., 1988). The longer isoform Drebrin A contains a unique insertion in the middle (Figure 1A) and is specifically expressed in adult neurons (hence called Drebrin A), whereas the E isoform (named after the embryonic Drebrin) is prominently expressed during the early stage of developing neurons and in various non-nervous tissues such as lung, intestine, and liver (Keon et al., 2000; Shirao and Obata, 1985). The N-terminal actin-depolymerizing factor homology (ADF-H) domain, although with no actin binding or depolymerizing activity, can bind to transcriptional regulator zinc-finger MYND-type containing 8 (ZMYND8), suggesting that Drebrin may play a regulatory role in cytoplasmic sequestering of ZMYND8 (Yamazaki et al., 2014; Yao et al., 2017). Following the ADF-H domain, Drebrin contains a putative coiled-coiled (CC) domain and a helical (HEL) domain that can bind to F-actin and promote actin bundle formation in a phosphorylation-dependent manner. It has been reported that Ser142 phosphorylation of Drebrin by cyclin-dependent kinase 5 relieves the autoinhibition of the CC domain, converting Drebrin from an F-actin binding protein to an F-actin bundling protein through the cooperation of HEL and CC domains (Ishikawa et al., 1994; Worth et al., 2013). In contrast to the highly conserved ADF-H domain and the actin binding region, the C terminus of Drebrin shows much lower sequence conservation and a lack of recognizable domains apart from two putative Homer binding motifs (HBMs) (Figure 1A). HBM contains a sequence motif of PPXXF, where X represents any amino acid. Drebrin HBMs were reported to interact with Homer2b *in vitro*, and the two proteins co-localize in synapses (Shiraishi-Yamaguchi et al., 2009; Shiraishi et al., 2003). However, the molecular mechanism and the physiological roles of this interaction remain poorly characterized.

Drebrin A is required for dendritic spine maturation and postsynaptic density-95 (PSD-95) accumulation at excitatory synapses. Downregulation of Drebrin A reduces synaptic localization of PSD-95 and clustering of F-actin at synapses, leading to reductions in the numbers and sizes of dendritic spines (Takahashi et al., 2003, 2006). However, overexpression of Drebrin A in cultured neurons induces abnormally long dendritic spines (Mizui et al., 2005). When expressed in various heterologous cells, Drebrin can induce formation of numerous filopodia (Shirao et al., 1992; Worth et al., 2013). Drebrin expression levels appear to decrease in Alzheimer's disease and Down syndrome patients, but increase in patients with various cancers (Dun and Chilton, 2010; Harigaya et al., 1996; Shim and Lubec, 2002; Xu et al., 2015). These studies suggest that Drebrin likely plays a role in dendritic spine development and in the pathogenesis of multiple diseases, possibly through regulating actin cytoskeletal organizations.

The Homer family scaffold proteins consists of three members, Homer1, 2, and 3, all of which have short and long

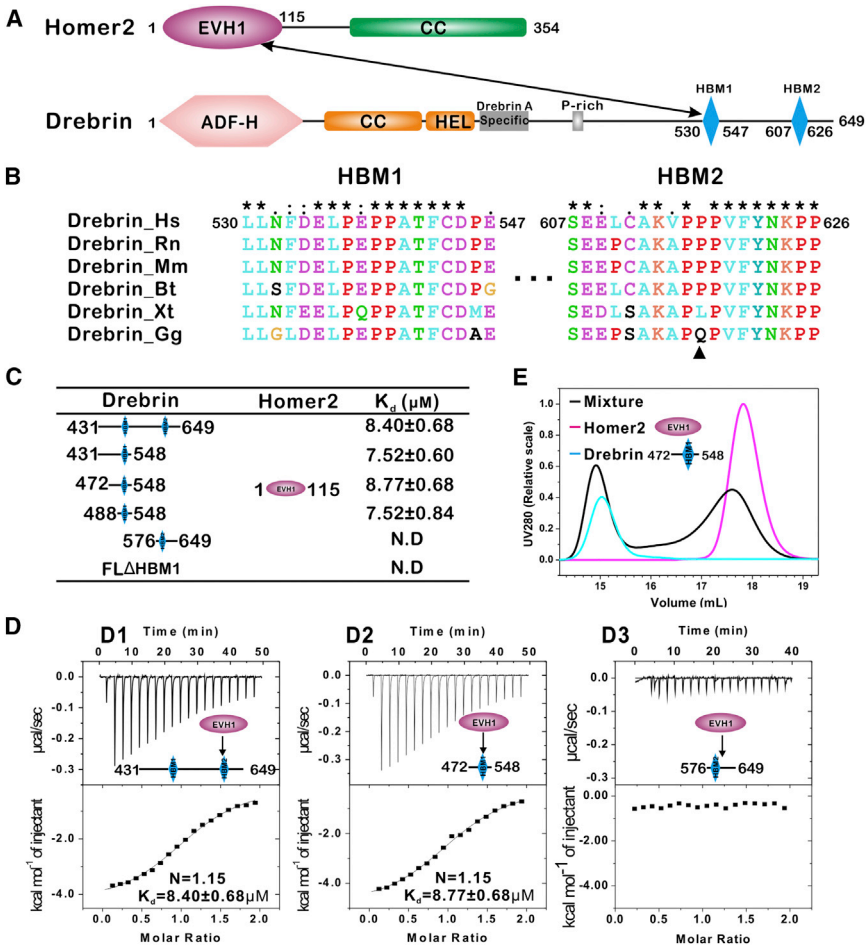

Figure 1. Biochemical Characterizations of the Homer2/Drebrin Interaction

(A) Domain organizations of Homer2 and Drebrin.

(B) Sequence alignment of a Drebrin tail showing the conserved HBM1 and the slightly less conserved HBM2. The black triangle shows the less-conserved proline in the second PPXXF motif. Mm, mouse; Rn, rat; Hs, human; Bt, cattle; Xt, *Xenopus tropicalis*; Gg, chicken.

(C and D) ITC-derived dissociation constants of various Drebrin proteins and Homer2 EVH1 (C). The mapping results show that Drebrin HBM1 (488–548) but not HBM2 can bind to Homer2 EVH1 with moderate affinity. N.D., not detectable. The ITC profiles are shown in (D) (Figure S1D): ITC-based measurements quantifying the binding affinities between Homer2 EVH1 and Drebrin tail 431–649 (left), Drebrin HBM1 472–548 (middle), or Drebrin HBM2 576–649 (right).

(E) Analytical gel filtration chromatography showing the binding profile of Homer2 EVH1 to Drebrin HBM1 472–548.

See also Figure S1.

isoforms generated by alternative splicing. Both longer and short forms contain an EVH1 domain, which can recognize various PPXXF motif-containing proteins, such as metabotropic glutamate receptors (mGluRs), Shank, Drebrin, inositol triphosphate receptor, and transient receptor potential canonical channels (Kammermeier and Worley, 2007; Shiraishi-Yamaguchi and Furuichi, 2007; Shiraishi-Yamaguchi et al., 2009). The crystal structure of the Homer1 EVH1/mGluR peptide (TPPSPF) complex reveals how Homer EVH1 recognizes the PPXXF motif (Beneken et al., 2000). However, there are more than 3,000 proteins (>10% of the total number of proteins) in the human proteome that contain the PPXXF motif. It is unlikely that all these proteins are true Homer binding partners. We reason that residues outside the PPXXF motifs may play a role in modulating their Homer EVH1 binding specificity. Besides the EVH1 domain, the longer isoforms of Homer also contain a CC region at the C terminus that forms an antiparallel tetramer. Homer tetramer and Shank form mesh-like structures capable of recruiting other synaptic proteins and promoting maturation of dendritic spines (Hayashi et al., 2009). The short monomeric isoforms of Homer, such as Homer1a, may modulate global synaptic scaling possibly by antagonizing the long tetrameric Homer during the wake/sleep cycle in mammals (de Vivo et al., 2017; Diering et al., 2017).

In this study, we solved the crystal structure of Homer EVH1 in complex with the extended first HBM (HBM1), revealing that the flanking sequences of the minimal HBM1 are important for Homer EVH1 binding. We further demonstrated that the Homer tetramer can promote the actin bundling activity of Drebrin to form thick actin bundles *in vitro*. In cells, the Homer tetramer augments filopodia elongation and the branching capacity of Drebrin. Finally, we showed that the monomeric Homer1a can effectively compete with the tetrameric Homer1b in binding to Drebrin and antagonize Homer1b-augmented actin bundling activity of Drebrin. Thus, the Homer/Drebrin interaction may play a role in the scaling of excitatory synapses by modulating synaptic actin cytoskeletons.

RESULTS

Homer EVH1 Domain Specifically Binds to the First PPXXF Motif of Drebrin

Detailed sequence analysis revealed that Drebrin contains two putative Homer EVH1 binding PPXXF motifs within its C-terminal tail (Figure 1A, denoted as HBM1 and HBM2 for Homer binding motifs 1 and 2). Both HBMs are quite conserved during evolution (Figure 1B). We first validated and quantified the interaction between Homer and Drebrin using the purified Homer2 EVH1 and the Drebrin C-terminal tail, which contains both putative HBMs. Isothermal titration calorimetry (ITC) experiments showed that the two proteins form a 1:1 complex with a K_d of ~8.4 μM (Figures 1C and 1D1). This indicates that only one HBM can bind to Homer2. To further characterize the above interaction, we divided the Drebrin C-terminal tail into two fragments, each containing one HBM as shown in Figures 1B and 1C. ITC analysis showed that Drebrin HBM1 binds

Table 1. Statistics of X-Ray Crystallographic Data Collection and Model Refinement

Data Collection	
Datasets	Homer-Drebrin
Space group	*P1*
Wavelength (Å)	0.9776
Unit cell parameters	
a, b, c (Å)	45.34, 47.81, 50.42
α, β, γ (°)	70.44, 83.56, 90.39
Resolution range (Å)	50–2.30 (2.34–2.30)
No. of unique reflections	17,008 (797)
Redundancy	3.5 (3.6)
I/σI	14.8 (1.8)
Completeness (%)	96.6. (94.5)
R_{merge}[a] (%)	6.4 (47.4)
$CC_{1/2}$ (last resolution shell)[b]	0.824
Structure Refinement	
Resolution (Å)	50–2.30 (2.44–2.30)
R_{cryst}[c]/R_{free}[d] (%)	19.16/22.82 (25.97/29.43)
RMSD	
Bonds (Å)	0.004
Angles (°)	0.782
Average B factor (Å^2)[e]	50.3
No. of atoms	
Protein atoms	2,938
Water	31
Ligands	0
No. of reflections	
Working set	16,171 (2,623)
Test set	821 (113)
Ramachandran plot regions (%)[e]	
Favored	98.4
Allowed	1.6
Outliers	0

Numbers in parentheses represent the value for the highest-resolution shell. RMSD, root-mean-square deviation.

[a] $R_{merge} = \Sigma|I_i - \langle I \rangle|/\Sigma I_i$, where I_i is the intensity of measured reflection and $\langle I \rangle$ is the mean intensity of all symmetry-related reflections.

[b] $CC_{1/2}$ were defined by Karplus and Diederichs (2012).

[c] $R_{cryst} = \Sigma||F_{calc}| - |F_{obs}||/\Sigma F_{obs}$, where F_{obs} and F_{calc} are observed and calculated structure factors.

[d] $R_{free} = \Sigma_T||F_{calc}| - |F_{obs}||/\Sigma F_{obs}$, where T is a test dataset of about 5% of the total unique reflections randomly chosen and set aside prior to refinement.

[e] B factors and Ramachandran plot statistics are calculated using MolProbity (Chen et al., 2010).

to Homer2 EVH1 at 1:1 stoichiometry, with the same affinity as the long tail that contains both HBMs (Figure 1D2), whereas no interaction was detected between Drebrin HBM2 and Homer2 EVH1 (Figure 1D3). Deleting HBM1 from the full-length Drebrin abolished its binding to Homer2 EVH1 (Figure 1C), indicating that HBM1 is the only Homer2 binding site of Drebrin. We further confirmed the ITC binding results using analytical gel filtration chromatography (Figures 1E and S1G). Finally, our ITC-based experiments showed that the EVH1 domains of Homer1, 2, and 3 all bind to Drebrin HBM1 with similar affinities (Figures 1D2, S1E, and S1F). This finding is expected given that the EVH1 domains of all Homer isoforms are extremely similar.

Structural Basis Governing the Specific Homer EVH1/Drebrin HBM1 Interaction

To understand how Homer EVH1 and Drebrin HBM1 interact at the atomic level, we solved the crystal structure of the Homer2 EVH1/Drebrin HBM1 complex by fusing the Drebrin HBM1 (amino acids [aa]: 530–550) to the C terminus of Homer2 EVH1 with a 15-aa flexible linker in between (Table 1). Drebrin HBM1 binds to the canonical hydrophobic pocket of Homer2 EVH1 domain (Figures 2A and 2B). The Pro (P539 and P540) and Phe (F543) residues of the PPXXF motif of Drebrin HBM1 occupy essentially the same positions as the corresponding residues of the mGluR5 PPXXF motif in the Homer1/mGluR5 complex (Figure 2C). Besides the well-defined PPXXF motif, there are clear densities in the F_o–F_c difference map indicating that residues flanking the PPXXF motif of Drebrin HBM1 also contribute to the interaction (Figures 2B and 2C).

The canonical PPXXF motif mainly binds to the Homer2 EVH1 domain via hydrophobic interactions (Figure 3A). Mutations of these critical residues significantly weakened the binding (Figure 3B). Of the flanking sequences, the side chain of $D545^D$ (the superscript denotes Drebrin) forms a critical hydrogen bond with the Homer2 $Q72^H$ (the superscript denotes Homer) backbone (Figure 3A). Substitution of $D545^D$ with Ala completely abolished the Drebrin/Homer2 interaction (Figure 3B), highlighting the importance of this side chain-main chain interaction. Multiple sequence alignments of reported Homer binders indicate that an Asp or Asn residue is preferred at this position (Figure 3C). At the N-terminal part of HBM1, hydrophobic interactions mediated by $P537^D$ and $W24^H$, $I16^H$ as well as $L536^D$ and $T68^H$, also contribute to the binding (Figure 3A). It is noted that the known Homer binders all contain a Leu (corresponding to $L536^D$) two or three residues preceding the PPXXF motif (Figure 3C).

Although both HBM1 and HBM2 contain the PPXXF motif, only HBM1 interacts with the Homer EVH1 domain (Figures 1 and 3D). We next set out to investigate the reason for this binding specificity. Since residues surrounding the PPXXF motif are quite different between HBM1 and HBM2 (Figure 3D), we first tested the impact on the binding by substituting each of those flanking residues in HBM1 to the corresponding sequence in HBM2. Surprisingly, the C544Y mutation abolished the EVH1 binding of HBM1 (Figures 3D and S2A), although $C544^D$ is not directly involved in the interaction (Figure 3A). We reasoned that a bulky residue Tyr at this position may sterically occlude $P539^D$ and thus prevent the PPXXF motif from adopting the proper conformation to interact with Homer. Consistent with this prediction, the C544F or C544W mutation also totally disrupted the Homer EVH1 binding of HBM1 (Figures S2B and S2C). Substitution of the N-terminal $L536^D$ to Ala or $P537^D$ to Lys decreased the binding affinity by a few folds, and mutation of $D545^D$ to Asn slightly weakened the binding (Figure 3D). We then tried to convert HBM2 into an HBM by introducing gain-of-function mutations based

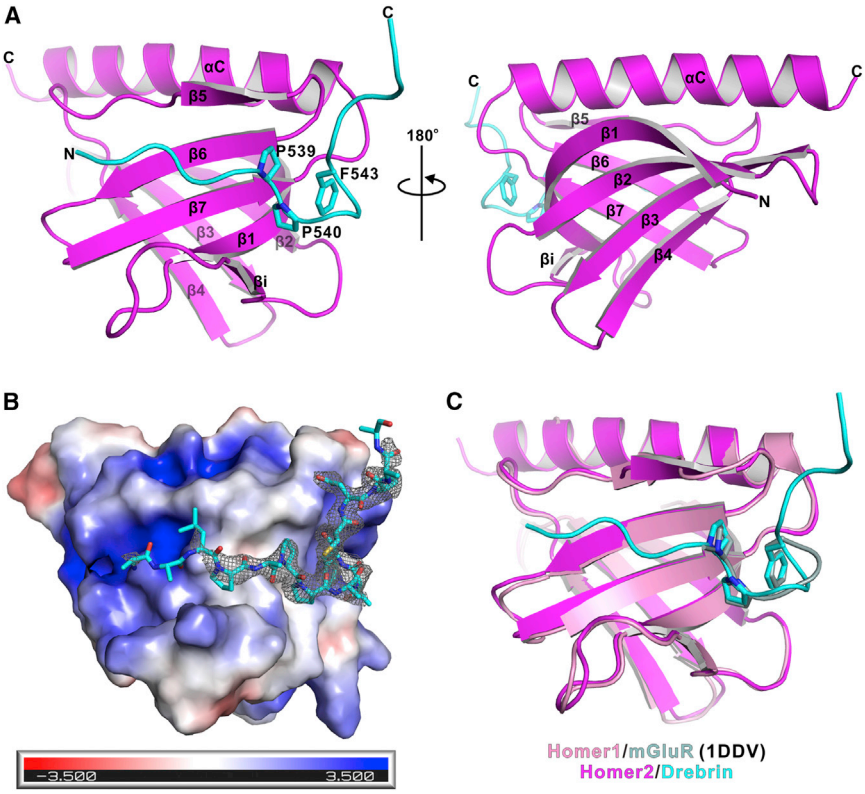

Figure 2. Overall Structure of the Homer EVH1/Drebrin HBM1 Complex

(A) Ribbon representation of the Homer2/Drebrin HBM1 complex structure. The Homer2 EVH1 domain is colored in magenta and the Drebrin HBM1 is colored in cyan. P539, P540, and F543 in the PPXXF motif are shown in the stick model.

(B) An omit map showing the Drebrin HBM1 (shown in stick model) binding to Homer2 EVH1 shown with the electrostatic potential surface. The F_o–F_c density map was generated by deleting the Drebrin HBM1 part from the final model and contoured at 3.0σ.

(C) Comparison of the Homer2 EVH1/Drebrin (magenta and cyan) and Homer1 EVH1/mGluR5 (pink and light-teal) structures.

on the above analysis. We found that the A613L, K614P, and Y622C triple mutation, but not the Y622C single-point mutation, could convert HBM2 into a weak Homer EVH1 binder (Figure 3D), reinforcing the conclusion that both the hydrophobic residue(s) preceding the PPXXF motif and a non-bulky aromatic residue immediately following the PPXXF motif play critical roles for the extended PPXXF motif to bind to Homer EVH1.

We further validated this conclusion by testing the bindings of mGluR1 or Shank3 to Homer EVH1 by ITC experiments. The binding affinity between mGluR1 and Homer2 was ~14 μM (Figures 3D and S3A), and mutation of L1150 (the hydrophobic Leu preceding the PPXXF motif) to Lys abolished this binding (Figures 3D and S3B). Stronger binding was observed between Shank3 and Homer2 (K_d ~0.84 μM) (Figures 3D and S3D), and substitution of L1806 with Lys weakened the interaction by about 5-fold (Figures 3D and S3E). In addition, mutation of the residue right after the PPXXF motif (highlighted by the red triangle in Figure 3C) in mGluR1 or Shank3 to bulky residue Tyr also dramatically decreased their Homer2 binding affinities (Figures 3D, S3C, and S3F). Taken together, our detailed structural and biochemical analyses reveal an extended PPXXF motif with a sequence pattern of **L**-X_{1-2}-**PPXXF**-Ω-(D/N), where X is any residue and Ω can be any residue but FYW, as the general Homer EVH1 binding motif.

Drebrin-Mediated Actin Bundling Activity Promoted by Homer Tetramerization and Phosphorylation

Recently, we showed that dimerization of Espin1 (an actin bundling protein) by binding to myosin III can facilitate the formation of Espin1-mediated thick actin bundles (Liu et al., 2016). Drebrin is monomeric (Figure S4A1) and was reported to be a weak actin bundling protein (Worth et al., 2013), and thus we speculated whether Homer binding-mediated Drebrin multimerization might be able to promote the actin bundling activity of Drebrin. To test this hypothesis, we first conducted a low-speed co-sedimentation assay, in which only the bundled F-actin could be spinned down with or without the purified Drebrin and Homer1b proteins. In the absence of Homer1b and Drebrin, no F-actin content was pelleted down when the sample was centrifuged at 10,000 × *g* for 20 min. Co-sedimentation results revealed that wild-type (WT) Drebrin alone exhibits weak F-actin bundling activity, which is significantly promoted by the addition of WT Homer1b (Figures 4A and 4C). Substitution of $W24^H$, a residue in Homer1b EVH1 essential for Drebrin binding, with Ala, eliminated Homer1b's ability to promote Drebrin-mediated actin bundling (Figures 3B, 4A and 4C). Correspondingly, removal of the PPATF motif from Drebrin also eliminated Homer1b binding-induced actin bundling by Drebrin (Figures 4A and 4C). To further test whether Homer tetramerization is required for promoting Drebrin-mediated actin bundling, we used purified Homer1a, an isoform of Homer1 lacking the C-terminal CC tetramerization domain. Interestingly, the co-sedimentation assay showed that the monomeric Homer1a was not capable of promoting Drebrin's actin bundling activity (Figures 4A and 4C). We next directly tested the role of the Homer1b tetramer on Drebrin's actin bundling activity by converting Homer1b into a dimer via substituting two hydrophobic residues (I332 and I337) in the CC domain of Homer1b with Arg and Glu, respectively (denoted as Homer1b II2RE). Consistent with an earlier study (Hayashi et al., 2009), the purified Homer1b II2RE stayed as a dimer in solution (Figure S4A2). Interestingly, the Homer1b II2RE mutant also has a weaker capacity in promoting Drebrin's actin bundling activity (Figures 4A and 4C). Taken together, our results suggest that tetramerization of Homer1b and the interaction between Drebrin and

A

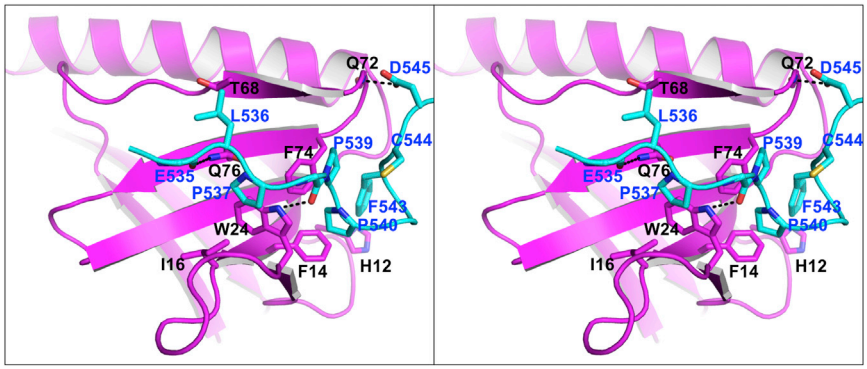

B

Drebrin 431-548	Homer2 EVH1	K_d(μM)
WT	WT	7.5±0.6
WT	W24A	N.D.
WT	F74A	~645
WT	G89A	~190
L536A	WT	19.8±3.3
P539A	WT	41.2±13.4
P540A	WT	N.D.
F543A	WT	N.D.
D545A	WT	N.D.

C

```
Drebrin   -DELPEPPATFCDPEE
mGluR5    LVALT-PPSPFRDSVD
IP3R      -GDLNNPPKKFRDCLF
Shank3    -IGLVPPPEEFANGIL
C/EBPβ    CLPLP-PPPAFKSMEV
RyR1      TTSLR-PPHHFSPPC-
consensus    LX1-2PPXXFΩ(D/N)
```

D

Protein	Sequence												K_d (μM)
Drebrin HBM1	L	P	E	P	P	A	T	F	C	D	P	E	7.5±0.6
Drebrin HBM2	A	K	A	P	P	P	V	F	Y	N	K	P	N.D.
Drebrin HBM1	A	P	E	P	P	A	T	F	C	D	P	E	19.8±3.3
	L	K	E	P	P	A	T	F	C	D	P	E	23.7±5.2
	L	P	A	P	P	A	T	F	C	D	P	E	3.1±0.4
	L	P	E	P	P	A	T	F	Y	D	P	E	N.D.
	L	P	E	P	P	A	T	F	C	N	P	E	19.5±4.0
	L	P	E	P	P	A	T	F	C	D	K	E	8.2±1.4
Drebrin HBM2	A	K	A	P	P	P	V	F	C	N	K	P	N.D.
	L	P	A	P	P	P	V	F	C	N	K	P	32.7±4.9
mGluR1 HBM	L	T	-	P	P	S	P	F	R	D	S	V	13.9±0.8
	K	T	-	P	P	S	P	F	R	D	S	V	N.D.
	L	T	-	P	P	S	P	F	Y	D	S	V	~100
Shank3 HBM	L	V	P	P	P	E	E	F	A	N	G	I	0.84±0.05
	K	V	P	P	P	E	E	F	A	N	G	I	4.44±0.14
	L	V	P	P	P	E	E	F	Y	N	G	I	9.9±1.2

Figure 3. The Detailed Homer EVH1/Drebrin HBM1 Interaction

(A) Stereo view of the detailed interaction between Homer2 EVH1 and Drebrin HBM1. Key residues are shown with the stick model. Hydrogen bonds are indicated with dashed lines.

(B) Summary of ITC-derived dissociation constants showing mutations of critical residues in the interface weakened or even abolished the binding between Homer2 EVH1 and Drebrin HBM1.

(C) Sequence alignment of reported Homer binding PPXXF containing protein. Critical residues in the PPXXF motif and peripheral regions (identified in this study) are highlighted in magenta and purple, respectively.

(D) Summary of ITC-derived dissociation constants of the bindings of Homer2 EVH1 to Drebrin HBM1/HBM2 inter-change mutants.

See also Figures S2 and S3.

Homer are both required for the enhanced actin bundling activity of Drebrin.

To exclude the possibility that Homer binding may allosterically regulate the actin bundling activities of Drebrin, we determined the binding affinities between Drebrin and F-actin with or without Homer1a via high-speed co-sedimentation assay (Figures S4B and S4C). Consistent with previous reported results, Drebrin binds to F-actin with a high affinity (K_d of WT ~0.2 μM and K_d of S142E ~0.1 μM) with a binding stoichiometry of ~1:5 (Grintsevich et al., 2010). Also, the binding affinity and binding stoichiometry are not changed significantly when Homer1a is added, suggesting that binding of Homer to the PPXXF motif does not affect the binding affinity of Drebrin to F-actin, which also indicates that the mechanism underlying the promotion of Drebrin's actin bundling activity by Homer1b is likely an avidity effect due to the multimerization of Drebrin instead of the allosteric regulation of Drebrin by Homer EVH1 binding.

Previous studies have shown that phosphorylation of Drebrin at S142 can regulate its actin bundling activity by releasing Drebrin autoinhibition (Worth et al., 2013). To test whether Drebrin phosphorylation can regulate actin bundling in the presence of Homer1b, we substituted S142 with Glu to mimic its phosphorylation. Drebrin S142E in complex with Homer1b showed a slight but significant increase of Drebrin's actin bundling activity in the low-speed co-sedimentation assay when compared with the WT Drebrin (Figures 4B and 4C).

To better investigate the impact of S142 phosphorylation on Drebrin's actin bundling activity, we used fluorescent microscopy (FM) and transmission electron microscopy (TEM) to directly visualize actin bundles induced by WT, S142A, and S142E Drebrin. The F-actin-only group showed background signal under FM, and nanometer-sized filaments under TEM (Figure 5A12). Consistent with the co-sedimentation results, Drebrin WT, S142A, or S142E mixed with F-actin showed faint fluorescence signal and very thin actin bundles under FM (Figures 5A1, 5A2, and 5A3), indicating that Drebrin WT/S142A/S142E alone exhibits very weak actin crosslinking activity. Strikingly, when Homer1b and Drebrin WT/S142A/S142E proteins were mixed with F-actin, long filamentous bundles could be observed under FM, and thick actin bundles were seen under TEM (Figures 5A3 and 5A4). We noted that the actin networks crosslinked by Homer1b and Drebrin WT/S142A were loose bundles with relative fluorescence intensity of ~0.168 ± 0.046/~0.163 ± 0.032 (Figures 5A4, 5A5, and 5B1). Interestingly, when incubated with the Homer1b and Drebrin S142E, F-actin formed compact and large bundles

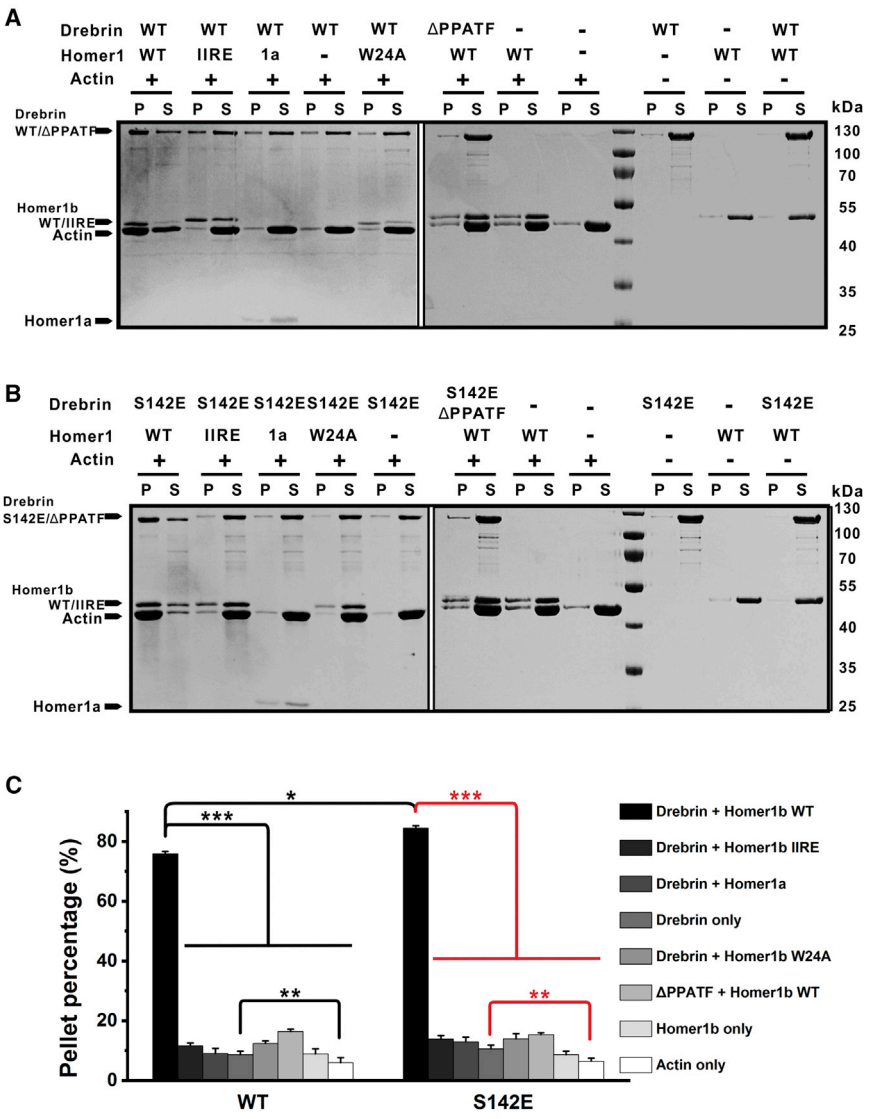

Figure 4. Homer1b Tetramer Promotes the Actin Bundling Activity of Drebrin

(A and B) Low-speed co-sedimentation assay of F-actin bundle formation with various Drebrin/Homer1 mixtures. "P" means pellets and "S" means supernatants. (A) Coomassie blue-stained SDS-PAGE of 4 μM F-actin incubated with 1 μM Drebrin WT with or without 1 μM Homer1. (B) Coomassie blue-stained SDS-PAGE of 4 μM F-actin incubated with 1 μM Drebrin S142E with or without 1 μM Homer1.

(C) Quantification of the percentage of actin in pellets from the different groups of experiments in (A and B). Values are expressed as means ± SD from three independent experiments and analyzed using independent sample t test.

*p < 0.05, **p < 0.01, ***p < 0.001. See also Figure S4.

with fluorescence intensities of ~0.289 ± 0.055 (Figures 5A6 and 5B1), indicating that phosphorylation at S142 of Drebrin can indeed further promote its actin bundling activity. As the control, Homer1b alone could not induce F-actin bundling (Figure 5A11). We also examined the actin network formed by Drebrin S142E + Homer1b II2RE (Figure 5A7), Drebrin S142E + Homer1a (Figure 5A8), as well as Drebrin S142E + Homer1b W24A (Figure 5A9) and Drebrin S142E ΔPPATF + Homer1b (Figure 5A10). The imaging results showed that F-actin in all these groups could only be crosslinked into thin bundles when compared with that induced by Drebrin S142E + Homer1b (Figure 5B2), further confirming the importance of Homer1b tetramerization and Drebrin/Homer interaction in promoting the actin bundling by Drebrin. The dimeric Homer1b II2RE displayed a higher actin bundle-promoting activity of Drebrin when compared with the monomeric Homer1a (Figure 5B), indicating that the level of Homer multimerization is positively correlated with its capacity in promoting the actin bundling activity of Drebrin.

Homer Tetramer Promotes Drebrin-Induced Formation of Filopodia

Drebrin can induce filopodia formation when expressed in various cells (Shirao et al., 1992; Worth et al., 2013). We speculated that the thick actin bundles assembled by the Drebrin/Homer complex *in vitro* may promote the formation and elongation of filopodia in cells. To test our hypothesis, we expressed various Drebrin and Homer1 constructs in COS7 cells and examined the morphology of filopodia by confocal microscopic imaging. When expressed in COS7 cells, Drebrin WT or S142E mutant induced the formation of numerous filopodia, whereas S142A mutant did not significantly induce filopodia formation (Figures 6A1, 6A2, and 6A3), as shown previously (Worth et al., 2013). Cells co-expressing Homer1b and Drebrin WT contained significantly more and longer filopodia compared with cells expressing Drebrin alone (Figure 6A4). Co-expression of Homer1b with the Drebrin S142E mutant further augmented the number and lengths of filopodia in these cells (Figures 6A5 and 6B). In contrast, the monomeric Homer1a could not promote filopodia formation, and the dimeric Homer1b II2RE mutant displayed a significantly weaker filopodia promotion activity when compared with Homer1b WT (Figures 6A7, 6A8, and 6B). Similarly, Homer1b W24A or Drebrin S142E ΔPPATF did not have any filopodia promotion activity in COS7 cells when compared with Drebrin S142E alone (Figures 6A9 and 6A10). Taken together, our cell-based assay results revealed that both Homer/Drebrin interaction and Homer tetramerization are important for the Drebrin-induced filopodia formation and elongation in COS7 cells.

Homer1a Can Antagonize Homer1b in Regulating Drebrin-Induced Actin Bundle Formation

Since the size of synapses is positively correlated with the amount of actin filaments in the synapse (Cingolani and

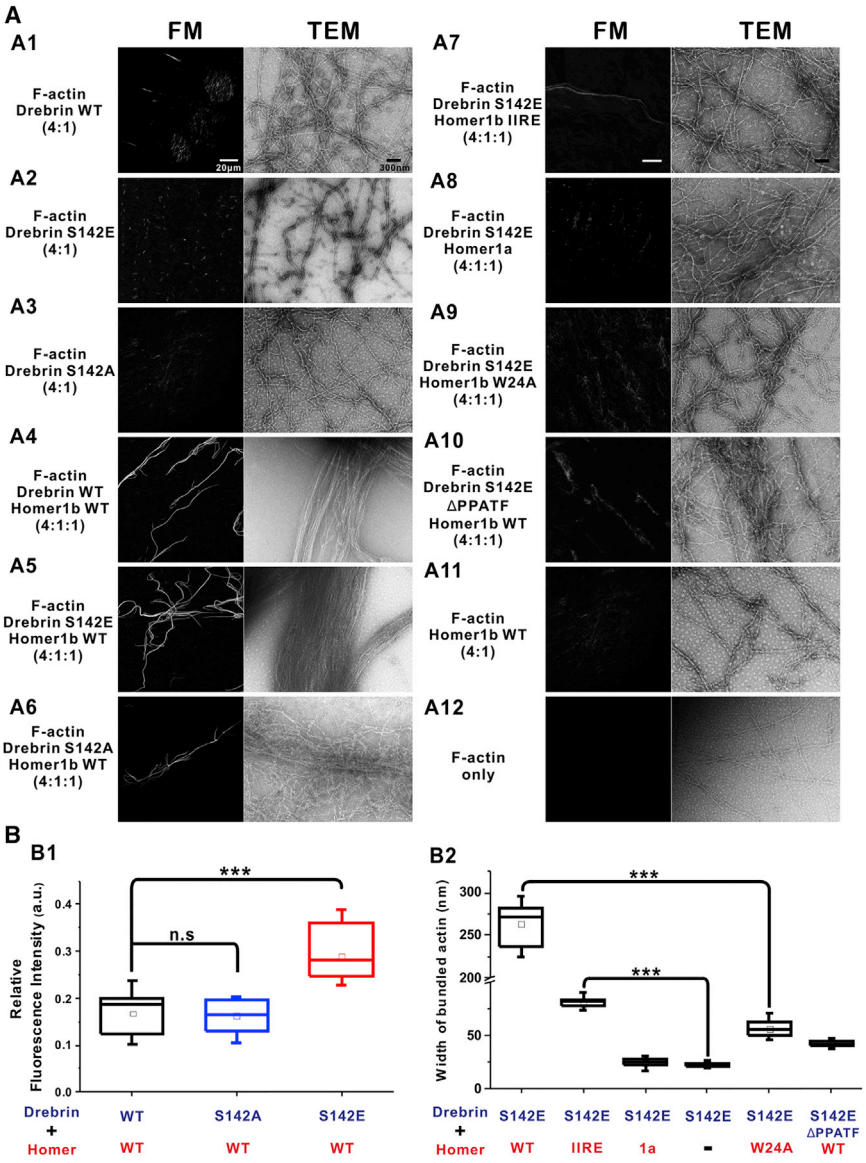

Figure 5. Phosphorylation of Drebrin at S142 Can Further Enhance the Actin Bundling Activity of Drebrin Mediated by Homer1b

(A) Representative confocal images (left) and transmission electron microscopy images (right) of F-actin induced by Drebrin with or without various forms of Homer1. (A1) Mixtures of F-actin and Drebrin WT at a 4:1 molar ratio; (A2) mixtures of F-actin and Drebrin S142E at a 4:1 molar ratio; (A3) mixtures of F-actin and Drebrin S142A at a 4:1 molar ratio; (A4) a 4:1:1 molar ratio mixture of F-actin + Drebrin WT + Homer1b WT; (A5) a 4:1:1 molar ratio mixture of F-actin + Drebrin S142E + Homer1b WT; (A6) a 4:1:1 molar ratio mixture of F-actin + Drebrin S142A + Homer1b WT; (A7) a 4:1:1 molar ratio mixture of F-actin + Drebrin S142E + Homer1b II2RE; (A8) a 4:1:1 molar ratio mixture of F-actin + Drebrin S142E + Homer1a; (A9) a 4:1:1 molar ratio mixture of F-actin + Drebrin S142E + Homer1b W24A; (A10) a 4:1:1 molar ratio mixture of F-actin + Drebrin S142E ΔPPATF + Homer1b WT; (A11) a 4:1 molar ratio mixture of F-actin + Homer1b WT; and (A12) F-actin only. The confocal images of A1-A12 are presented at the same noise level. Note that the fluorescence signal of F-actin only in A12 is near the background level. Scale bar of FM: 20 μm. Scale bar of TEM: 300 nm.

(B) Quantification results showing that tetramerization of Homer can enhance the actin bundling activities of Drebrin. (B1) Quantitative analysis of the relative fluorescence intensities of F-actin bundles in (A4), black; (A5), red; and (A6), blue; (B2) Quantitative analysis of the bundle width of S142E mutant group.

Statistics were performed by independent sample t test. n.s., not significant, ***$p < 0.001$.

DISCUSSION

An earlier study suggested that Drebrin contains two potential Homer binding sites with the PPXXF motif in its C-terminal tail (Shiraishi-Yamaguchi et al., 2009). In this study, we demonstrate that Homer EVH1 specifically binds to an extended sequence encompassing the first PPXXF motif, instead of the second PPXXF sequence-containing site. We further defined an extended Homer EVH1 binding motif with the consensus sequence of **L**-X_{1-2}-**PPXXF**-Ω-(D/N), where X is any residue and Ω can be any residue but F/Y/W. The structure of Homer EVH1 in complex with the extended PPXXF motif of Drebrin, together with detailed biochemical studies, elucidated the molecular mechanism governing this specific interaction.

The long isoforms of Homer such as Homer1b contain a C-terminal CC tetramerization domain. Each Homer tetramer can crosslink four Drebrin molecules. Thus, the tetrameric Homer can function as an organization hub to enable its bound Drebrin to crosslink actin filaments via its N-terminal actin binding domain (Figure 7E). As such, the Homer tetramer can promote the actin bundling activity of Drebrin.

Goda, 2008; Ethell and Pasquale, 2005; Hotulainen and Hoogenraad, 2010; Kim et al., 2015; Okamoto et al., 2009), we speculated that Homer1a might be able to antagonize Homer1b to modulate Drebrin-induced actin bundle formation. To test this hypothesis, we added increasing amounts of Homer1a into a Homer1b/Drebrin mixture at a fixed concentration and assayed the actin bundle formation by co-sedimentation (Figures 7A and 7C) and imaging-based assays (Figures 7B and 7D). In the absence of Homer1a, the vast majority of actin formed F-actin filaments when incubated with the Homer1b/Drebrin mixture in the co-sedimentation and FM imaging assays (Figure 7). Expectedly, the addition of Homer1a disassembled Homer1b/Drebrin-induced actin bundles in a dose-dependent manner in both co-sedimentation and FM imaging assays (Figure 7), presumably due to the displacement of the tetrameric Homer1b from Drebrin by the monomeric Homer1a (Figure 7E).

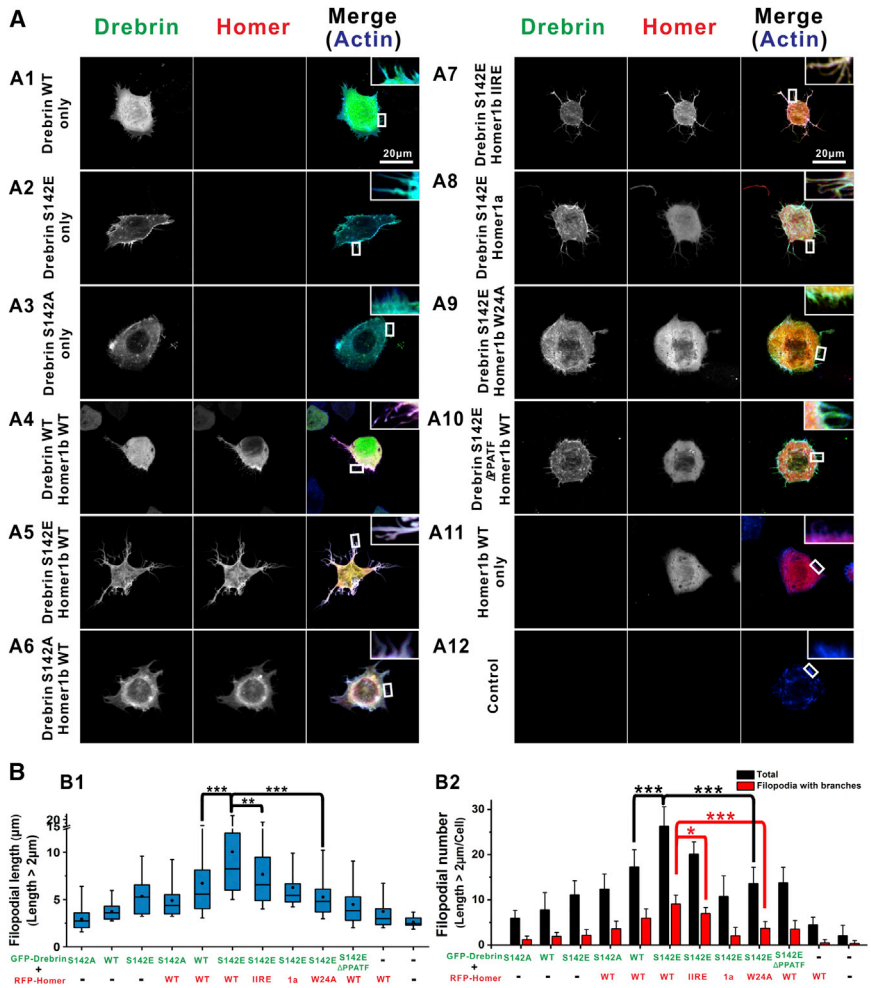

Figure 6. Drebrin/Homer Tetramer Interaction Promotes Both Number and Length of Filopodia Formation in COS7 Cells

(A) Representative confocal images of COS7 cells transfected with GFP-Drebrin and each individual forms of RFP-Homer1 (A1–A12). Actin filaments are stained with phalloidin. (A1) Drebrin WT; (A2) Drebrin S142E; (A3) Drebrin S142A; (A4) Drebrin WT + Homer1b WT; (A5) Drebrin S142E + Homer1b WT; (A6) Drebrin S142A + Homer1b WT; (A7) Drebrin S142E + Homer1b II2RE; (A8) Drebrin S142E + Homer1a; (A9) Drebrin S142E + Homer1b W24A; (A10) Drebrin S142E ΔPPATF + Homer1b WT; (A11) Homer1b WT; and (A12) negative control without any transfection. Scale bar: 20 μm.

(B) Quantification of filopodial length (B1) and filopodial number per cell (B2). A protrusion with a length >2 μm is defined as a filopodia. Values are expressed in boxplot or means ± SD from three independent experiments with 20 cells per experiment, analyzed using independent sample t test.

*$p < 0.05$, **$p < 0.01$, ***$p < 0.001$. Note: For A1, A2 and A3, Homer were not transfected as indicated (therefore no signal was detected in these panels). For A11, Drebrin was not transfected (thus no signal was observed).

Formation of actin bundles is often facilitated by actin filament crosslinking proteins. Intuitively, such actin filament crosslinking proteins usually contain multiple actin binding domains, either with one single chain or via forming oligomers (Bartles, 2000; Okamoto et al., 2007; Winder and Ayscough, 2005). Actin bundles assembled by monomeric proteins with only one actin binding domain usually have limited sizes (Claessens et al., 2008). Here we showed that, instead of forming homo-oligomers, monomeric Drebrin functions to bundle actin filaments via Homer-mediated oligomerization. Target protein binding-mediated multimerization of monomeric actin bundling proteins might be a general mechanism for these proteins to regulate their actin bundling activities. For example, crosslinking of Espin1, another monomeric actin bundling protein, by myosin III has also been shown to promote its actin bundling activity (Liu et al., 2016). An obvious advantage of this strategy is that their actin bundling activity can be regulated by their target proteins.

Homer is an important and highly abundant scaffold protein in dendritic spines. Elevated expression of the tetrameric Homer in neurons is known to promote dendritic spine formation and increase synaptic strength (Hayashi et al., 2009; Sala et al., 2001). Conversely, overexpression of the monomeric isoform of Homer has been shown to cause spine shrinkage and weaken synaptic strength (de Vivo et al., 2017; Diering et al., 2017; Sala et al., 2003). It is well established that enlarged dendritic spines are positively correlated with more crosslinked actin filaments in spines (Kim et al., 2015; Koskinen and Hotulainen, 2014; Okamoto et al., 2007, 2009). Homer1a was reported to regulate synapse function in a neuronal activity-dependent manner, but Homer1b did not show the same activity (Brakeman et al., 1997; Kato et al., 1997). In addition, it has been shown recently that the monomeric Homer1a is dramatically upregulated during the sleeping period in the wake/sleep cycles of mice, and the massive Homer1a upregulation is correlated with the global synapse downscaling of neurons from the cortex (de Vivo et al., 2017; Diering et al., 2017). In this study, we demonstrate that the monomeric Homer1a can directly antagonize tetrameric Homer1b to downregulate the actin bundling activity of Drebrin (Figure 7). The discovery of Homer1a-mediated actin bundle disassembly, via displacement of tetrameric Homer1b from Drebrin, may be a possible mechanism underlying the Homer1a-induced synaptic downscaling during the sleeping period in animal brains.

Three general Pro-rich motif (PRM) binding domains are currently known: the Src-homology 3 domains (SH3 domains), the WW domains, the EVH1 domains. Other PRM binding modules include the single-domain protein profilin, the GYF domain from CD2 binding protein 2, and the ubiquitin E2 variant domain from viral Gag protein (Ball et al., 2005; Li, 2005) (Figure 8A). A general feature for the PRM recognition mode is that the PRM usually forms a polyproline II helix to dock into the

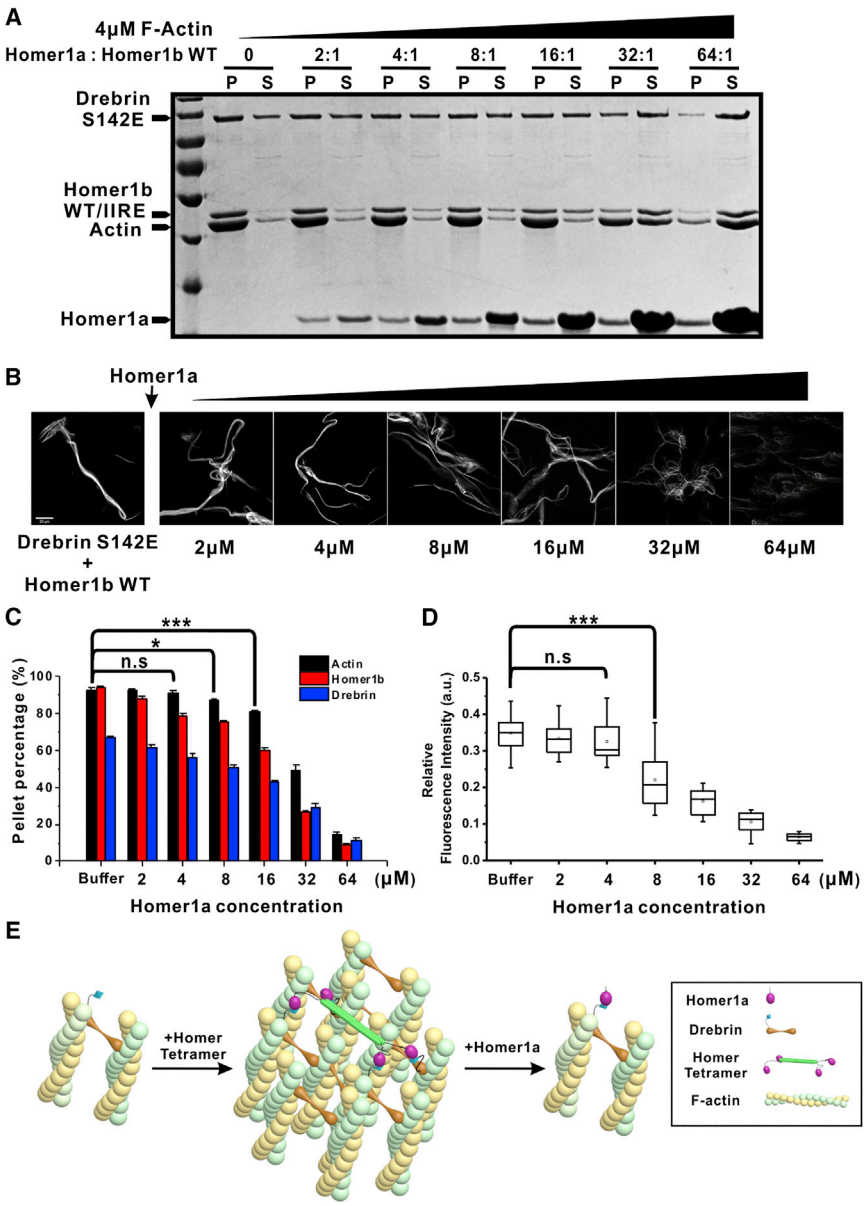

Figure 7. Homer1a Antagonizes Homer1b in Promoting the Actin Bundling Activity of Drebrin

(A) SDS-PAGE analysis of low-speed co-sedimentation assay of the Homer1a/Homer1b competition assay. In this assay. Homer1b was fixed at 1 μM, and Homer1a was increased from 0 to 64 μM as indicated. P, pellets; S, supernatants.

(B) Representative confocal images of F-actin induced by Drebrin S142E and Homer1b with/without various ratios of Homer1a. Mixtures of F-actin/Drebrin S142E/Homer1b without Homer1a (left); mixtures of F-actin/Drebrin S142E/Homer1b with Homer1a at the Homer1a:Homer1b ratios of 2:1, 4:1, 8:1, 16:1, 32:1, and 64:1, respectively (right). Scale bar: 20 μm.

(C) Quantification results of the assay showing the bundled F-actin can be disassembled by increasing concentrations of competing Homer1a.

(D) Quantitative analysis of the relative fluorescence intensities of F-actin bundles with various ratio of Homer1a added to the mixture. Values are expressed as means ± SD or boxplot from three independent experiments and analyzed using independent sample t test. n.s., not significant, *$p < 0.05$, ***$p < 0.001$.

(E) Schematic cartoon showing Homer tetramer-mediated higher-order actin bundling by Drebrin. Without Homer, Drebrin can induce formation of thin F-actin bundles (left). The Homer tetramer can crosslink Drebrin and further increase the actin bundling activity of Drebrin, thus promoting even thicker actin bundle formation (middle). The Homer monomer, Homer1a can antagonize Homer1b to modulate Drebrin-induced actin bundle formation (right).

hydrophobic groove formed by a number of aromatic residues (Figures 8B–8E). Furthermore, some non-proline residues (charged or hydrophobic) outside of the core PRM are critical for the interaction between PRM and PRM binding domains. For example, the Arg in the SH3 binding motif can form a salt bridge with a Glu from the SH3 domain (Feng et al., 1994; Li et al., 2018) (Figure 8B). The Tyr in the "PPxY" is involved in hydrogen bonding with the conserved His from the class I WW domain (Huang et al., 2000) (Figure 8C1). The Phe in the class I EVH1 binding motif form a cation-π interaction with the Arg from the EVH1 domain (Prehoda et al., 1999) (Figure 8D1). In the current study, we showed the importance of the flanking sequence of PRM (e.g., $D545^{D}$; Figures 3 and 8D2) for Drebrin to bind to Homer EVH1. With such distinct features, PRM binding domains can achieve target binding specificity albeit with moderate binding affinities, a property suited for dynamic regulations in signal transductions.

STAR★METHODS

Detailed methods are provided in the online version of this paper and include the following:

- KEY RESOURCES TABLE
- CONTACT FOR REAGENT AND RESOURCE SHARING
- EXPERIMENTAL MODEL AND SUBJECT DETAILS
  - COS7 Cells Culture
- METHOD DETAILS
  - Constructs and Protein Purification
  - Isothermal Titration Calorimetry (ITC) Assay

A

Domain and Class		PRM motif	Examples
SH3 domain			
	Class I	(R/K)pΦPxΦP	Src, Yes, Abl, PI3K
	Class II	PpΦPΦ(R/K)	Src, PLCγ, Nck, Cortactin
	Atypical	PxPxxRHxx(R/H/K)	CIN85
WW domain			
	Class I	PPxY	Dystrophin, YAP, ITCH, Smurf2
	Class II	poly-Pro	FE65, PRPF40A
EVH1 domain			
	Class I	FPxΦP	Mena, VASP
	Class II	Lx_{1-2}PPxxFΩ(D/N)	Homer1,2,3
Profilin		poly-Pro	Profilin

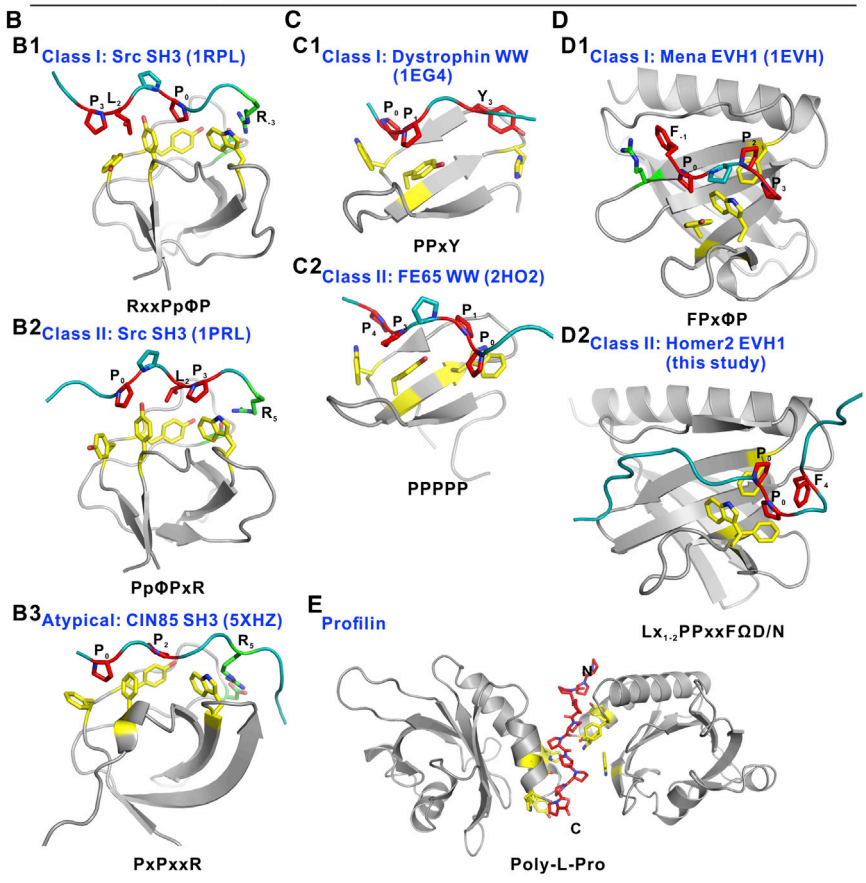

Figure 8. Comparison of the Different Interfaces of PRM Binding Modules

(A) Summary of different binding domains for PRM-containing motifs. Φ, x, and Ω represent hydrophobic, any amino acid residue and any residue but YFW, respectively. Lower-case letters represent the residue is favored at this position.

(B–E) The detailed interactions of representative members of each PRM binding family with their proline-rich ligands. Yellow, residues which form the base of binding surface; red, residues of ligand which have close hydrophobic contacts with the PRM domain; green, variable residues that have contacts with ligand. The first proline residue that makes close hydrophobic contact in the ligand is assigned the number zero. (B) SH3 domain, (C) WW domain, (D) EVH1 domain, and (E) profilin.

SUPPLEMENTAL INFORMATION

Supplemental Information includes four figures and can be found with this article online at https://doi.org/10.1016/j.str.2018.10.011.

ACKNOWLEDGMENTS

We thank the Shanghai Synchrotron Radiation Facility (SSRF) BL17U1 and BL19U1 for X-ray beam time. We also thank the Life Science Research Center, Southern University of Science and Technology (SUSTech) for TEM time. This work was supported by grants from the Minister of Science and Technology of China (2014CB910204), the National Key R&D Program of China (2016YFA0501903), the Natural Science Foundation of Guangdong Province (2016A030312016), and Shenzhen Basic Research Grant (JCYJ20160229153100269) (to M.Z.), grants from the National Natural Science Foundation of China (31670765) and Shenzhen Basic Research Grants (JCYJ20160427185712266 and JCYJ20170411090807530) (to W.L.), and a grant from the National Natural Science Foundation of China (no. 31700673)

(to H.L.). M.Z. is a Kerry Holdings Professor in Science and a Senior Fellow of IAS at HKUST.

AUTHOR CONTRIBUTIONS

H.L., J.L., W.L., J.W., and M.Z. designed the experiments. Z.L., H.L., and Q.Y. performed biochemistry and cell biology experiments. J.L. is responsible for the structural biology experiments. Y.L., H.Y., and C.Y. are responsible for the TEM imaging experiments. All authors analyzed the results. Z.L., H.L., J.L., Z.F., W.L., and M.Z. wrote the manuscript. M.Z. coordinated the research.

DECLARATION OF INTERESTS

The authors declare no competing interests.

Received: May 31, 2018
Revised: August 26, 2018
Accepted: October 18, 2018
Published: November 29, 2018

REFERENCES

Adams, P.D., Afonine, P.V., Bunkoczi, G., Chen, V.B., Davis, I.W., Echols, N., Headd, J.J., Hung, L.W., Kapral, G.J., Grosse-Kunstleve, R.W., et al. (2010). PHENIX: a comprehensive Python-based system for macromolecular structure solution. Acta Crystallogr. D Biol. Crystallogr. *66*, 213–221.

Ball, L.J., Kuhne, R., Schneider-Mergener, J., and Oschkinat, H. (2005). Recognition of proline-rich motifs by protein-protein-interaction domains. Angew. Chem. Int. Ed. *44*, 2852–2869.

Bartles, J.R. (2000). Parallel actin bundles and their multiple actin-bundling proteins. Curr. Opin. Cell Biol. *12*, 72–78.

Beneken, J., Tu, J.C., Xiao, B., Nuriya, M., Yuan, J.P., Worley, P.F., and Leahy, D.J. (2000). Structure of the Homer EVH1 domain-peptide complex reveals a new twist in polyproline recognition. Neuron *26*, 143–154.

Brakeman, P.R., Lanahan, A.A., O'Brien, R., Roche, K., Barnes, C.A., Huganir, R.L., and Worley, P.F. (1997). Homer: a protein that selectively binds metabotropic glutamate receptors. Nature *386*, 284–288.

Chen, V.B., Arendall, W.B., 3rd, Headd, J.J., Keedy, D.A., Immormino, R.M., Kapral, G.J., Murray, L.W., Richardson, J.S., and Richardson, D.C. (2010). MolProbity: all-atom structure validation for macromolecular crystallography. Acta Crystallogr. D Biol. Crystallogr. *66*, 12–21.

Cingolani, L.A., and Goda, Y. (2008). Actin in action: the interplay between the actin cytoskeleton and synaptic efficacy. Nat. Rev. Neurosci. *9*, 344–356.

Claessens, M.M., Semmrich, C., Ramos, L., and Bausch, A.R. (2008). Helical twist controls the thickness of F-actin bundles. Proc. Natl. Acad. Sci. U S A *105*, 8819–8822.

de Vivo, L., Bellesi, M., Marshall, W., Bushong, E.A., Ellisman, M.H., Tononi, G., and Cirelli, C. (2017). Ultrastructural evidence for synaptic scaling across the wake/sleep cycle. Science *355*, 507–510.

Diering, G.H., Nirujogi, R.S., Roth, R.H., Worley, P.F., Pandey, A., and Huganir, R.L. (2017). Homer1a drives homeostatic scaling-down of excitatory synapses during sleep. Science *355*, 511–515.

Dun, X.P., and Chilton, J.K. (2010). Control of cell shape and plasticity during development and disease by the actin-binding protein Drebrin. Histol. Histopathol. *25*, 533–540.

Emsley, P., Lohkamp, B., Scott, W.G., and Cowtan, K. (2010). Features and development of Coot. Acta Crystallogr. D Biol. Crystallogr. *66*, 486–501.

Ethell, I.M., and Pasquale, E.B. (2005). Molecular mechanisms of dendritic spine development and remodeling. Prog. Neurobiol. *75*, 161–205.

Feng, S., Chen, J.K., Yu, H., Simon, J.A., and Schreiber, S.L. (1994). Two binding orientations for peptides to the Src SH3 domain: development of a general model for SH3-ligand interactions. Science *266*, 1241–1247.

Grintsevich, E.E., Galkin, V.E., Orlova, A., Ytterberg, A.J., Mikati, M.M., Kudryashov, D.S., Loo, J.A., Egelman, E.H., and Reisler, E. (2010). Mapping of drebrin binding site on F-actin. J. Mol. Biol. *398*, 542–554.

Harigaya, Y., Shoji, M., Shirao, T., and Hirai, S. (1996). Disappearance of actin-binding protein, drebrin, from hippocampal synapses in Alzheimer's disease. J. Neurosci. Res. *43*, 87–92.

Hayashi, M.K., Tang, C., Verpelli, C., Narayanan, R., Stearns, M.H., Xu, R.M., Li, H., Sala, C., and Hayashi, Y. (2009). The postsynaptic density proteins Homer and Shank form a polymeric network structure. Cell *137*, 159–171.

Hotulainen, P., and Hoogenraad, C.C. (2010). Actin in dendritic spines: connecting dynamics to function. J. Cell Biol. *189*, 619–629.

Huang, X., Poy, F., Zhang, R., Joachimiak, A., Sudol, M., and Eck, M.J. (2000). Structure of a WW domain containing fragment of dystrophin in complex with beta-dystroglycan. Nat. Struct. Biol. *7*, 634–638.

Ishikawa, R., Hayashi, K., Shirao, T., Xue, Y., Takagi, T., Sasaki, Y., and Kohama, K. (1994). Drebrin, a development-associated brain protein from rat embryo, causes the dissociation of tropomyosin from actin filaments. J. Biol. Chem. *269*, 29928–29933.

Kammermeier, P.J., and Worley, P.F. (2007). Homer 1a uncouples metabotropic glutamate receptor 5 from postsynaptic effectors. Proc. Natl. Acad. Sci. U S A *104*, 6055–6060.

Karplus, P.A., and Diederichs, K. (2012). Linking crystallographic model and data quality. Science *336*, 1030–1033.

Kato, A., Ozawa, F., Saitoh, Y., Hirai, K., and Inokuchi, K. (1997). vesl, a gene encoding VASP/Ena family related protein, is upregulated during seizure, long-term potentiation and synaptogenesis. FEBS Lett. *412*, 183–189.

Keon, B.H., Jedrzejewski, P.T., Paul, D.L., and Goodenough, D.A. (2000). Isoform specific expression of the neuronal F-actin binding protein, drebrin, in specialized cells of stomach and kidney epithelia. J. Cell Sci. *113* (Pt 2), 325–336.

Kim, K., Lakhanpal, G., Lu, H.E., Khan, M., Suzuki, A., Hayashi, M.K., Narayanan, R., Luyben, T.T., Matsuda, T., Nagai, T., et al. (2015). A temporary gating of actin remodeling during synaptic plasticity consists of the interplay between the kinase and structural functions of CaMKII. Neuron *87*, 813–826.

Kojima, N., Shirao, T., and Obata, K. (1993). Molecular cloning of a developmentally regulated brain protein, chicken drebrin A and its expression by alternative splicing of the drebrin gene. Brain Res. Mol. Brain Res. *19*, 101–114.

Koskinen, M., and Hotulainen, P. (2014). Measuring F-actin properties in dendritic spines. Front. Neuroanat. *8*, 74.

Li, Q., Yang, W., Wang, Y., and Liu, W. (2018). Biochemical and structural studies of the interaction between ARAP1 and CIN85. Biochemistry *57*, 2132–2139.

Li, S.S. (2005). Specificity and versatility of SH3 and other proline-recognition domains: structural basis and implications for cellular signal transduction. Biochem. J. *390*, 641–653.

Liu, H., Li, J., Raval, M.H., Yao, N., Deng, X., Lu, Q., Nie, S., Feng, W., Wan, J., Yengo, C.M., et al. (2016). Myosin III-mediated cross-linking and stimulation of actin bundling activity of Espin. Elife *5*, https://doi.org/10.7554/eLife.12856.

Mahoney, N.M., Janmey, P.A., and Almo, S.C. (1997). Structure of the profilin-poly-L-proline complex involved in morphogenesis and cytoskeletal regulation. Nat. Struct. Biol. *4*, 953–960.

McCoy, A.J., Grosse-Kunstleve, R.W., Adams, P.D., Winn, M.D., Storoni, L.C., and Read, R.J. (2007). Phaser crystallographic software. J. Appl. Crystallogr. *40*, 658–674.

Meiyappan, M., Birrane, G., and Ladias, J.A. (2007). Structural basis for polyproline recognition by the FE65 WW domain. J. Mol. Biol. *372*, 970–980.

Mizui, T., Takahashi, H., Sekino, Y., and Shirao, T. (2005). Overexpression of drebrin A in immature neurons induces the accumulation of F-actin and PSD-95 into dendritic filopodia, and the formation of large abnormal protrusions. Mol. Cell. Neurosci. *30*, 149–157.

Okamoto, K., Bosch, M., and Hayashi, Y. (2009). The roles of CaMKII and F-actin in the structural plasticity of dendritic spines: a potential molecular identity of a synaptic tag? Physiology (Bethesda) *24*, 357–366.

Okamoto, K., Narayanan, R., Lee, S.H., Murata, K., and Hayashi, Y. (2007). The role of CaMKII as an F-actin-bundling protein crucial for maintenance of dendritic spine structure. Proc. Natl. Acad. Sci. U S A *104*, 6418–6423.

Otwinowski, Z., and Minor, W. (1997). Processing of X-ray diffraction data collected in oscillation mode. Methods Enzymol. *276*, 307–326.

Prehoda, K.E., Lee, D.J., and Lim, W.A. (1999). Structure of the enabled/VASP homology 1 domain-peptide complex: a key component in the spatial control of actin assembly. Cell *97*, 471–480.

Sala, C., Futai, K., Yamamoto, K., Worley, P.F., Hayashi, Y., and Sheng, M. (2003). Inhibition of dendritic spine morphogenesis and synaptic transmission by activity-inducible protein Homer1a. J. Neurosci. *23*, 6327–6337.

Sala, C., Piech, V., Wilson, N.R., Passafaro, M., Liu, G., and Sheng, M. (2001). Regulation of dendritic spine morphology and synaptic function by Shank and Homer. Neuron *31*, 115–130.

Shim, K.S., and Lubec, G. (2002). Drebrin, a dendritic spine protein, is manifold decreased in brains of patients with Alzheimer's disease and Down syndrome. Neurosci. Lett. *324*, 209–212.

Shiraishi-Yamaguchi, Y., and Furuichi, T. (2007). The Homer family proteins. Genome Biol. *8*, 206.

Shiraishi-Yamaguchi, Y., Sato, Y., Sakai, R., Mizutani, A., Knopfel, T., Mori, N., Mikoshiba, K., and Furuichi, T. (2009). Interaction of Cupidin/Homer2 with two actin cytoskeletal regulators, Cdc42 small GTPase and Drebrin, in dendritic spines. BMC Neurosci. *10*, 25.

Shiraishi, Y., Mizutani, A., Mikoshiba, K., and Furuichi, T. (2003). Coincidence in dendritic clustering and synaptic targeting of homer proteins and NMDA receptor complex proteins NR2B and PSD95 during development of cultured hippocampal neurons. Mol. Cell. Neurosci. *22*, 188–201.

Shirao, T., Kojima, N., Kato, Y., and Obata, K. (1988). Molecular cloning of a cDNA for the developmentally regulated brain protein, drebrin. Brain Res. *464*, 71–74.

Shirao, T., Kojima, N., and Obata, K. (1992). Cloning of drebrin A and induction of neurite-like processes in drebrin-transfected cells. Neuroreport *3*, 109–112.

Shirao, T., and Obata, K. (1985). Two acidic proteins associated with brain development in chick embryo. J. Neurochem. *44*, 1210–1216.

Takahashi, H., Mizui, T., and Shirao, T. (2006). Down-regulation of drebrin A expression suppresses synaptic targeting of NMDA receptors in developing hippocampal neurones. J. Neurochem. *97* (*Suppl 1*), 110–115.

Takahashi, H., Sekino, Y., Tanaka, S., Mizui, T., Kishi, S., and Shirao, T. (2003). Drebrin-dependent actin clustering in dendritic filopodia governs synaptic targeting of postsynaptic density-95 and dendritic spine morphogenesis. J. Neurosci. *23*, 6586–6595.

Winder, S.J., and Ayscough, K.R. (2005). Actin-binding proteins. J. Cell Sci. *118*, 651–654.

Worth, D.C., Daly, C.N., Geraldo, S., Oozeer, F., and Gordon-Weeks, P.R. (2013). Drebrin contains a cryptic F-actin-bundling activity regulated by Cdk5 phosphorylation. J. Cell Biol. *202*, 793–806.

Xu, S.Q., Buraschi, S., Morcavallo, A., Genua, M., Shirao, T., Peiper, S.C., Gomella, L.G., Birbe, R., Belfiore, A., Iozzo, R.V., et al. (2015). A novel role for drebrin in regulating progranulin bioactivity in bladder cancer. Oncotarget *6*, 10825–10839.

Yamazaki, H., Kojima, N., Kato, K., Hirose, E., Iwasaki, T., Mizui, T., Takahashi, H., Hanamura, K., Roppongi, R.T., Koibuchi, N., et al. (2014). Spikar, a novel drebrin-binding protein, regulates the formation and stabilization of dendritic spines. J. Neurochem. *128*, 507–522.

Yao, N., Li, J., Liu, H., Wan, J., Liu, W., and Zhang, M. (2017). The structure of the ZMYND8/Drebrin complex suggests a cytoplasmic sequestering mechanism of ZMYND8 by Drebrin. Structure *25*, 1657–1666.e3.

STAR★METHODS

KEY RESOURCES TABLE

REAGENT or RESOURCE	SOURCE	IDENTIFIER
Chemicals, Peptides, and Recombinant Proteins		
Rabbit skeletal muscle actin	Cytoskeleton, Inc.	Cat#AKL99
Dulbecco's Modified Eagle Medium (DMEM)	Thermo Fisher Scientific	Cat#11995065
Alexa Fluor™ 555 Phalloidin	Thermo Fisher Scientific	Cat#A34055
Alexa Fluor™ 647 Phalloidin	Thermo Fisher Scientific	Cat#A22287
fetal bovine serum (FBS)	Thermo Fisher Scientific	Cat#16000044
penicillin-streptomycin	Thermo Fisher Scientific	Cat#15140122
Recombinant protein: Human Drebrin WT (aa: M1-D649, ref# NM_004395.3)	This paper	N/A
Recombinant protein: Mouse Homer1b WT (aa: M1-S354, ref# NM_001284189.2)	This paper	N/A
Recombinant protein: Mouse Homer1a (aa: M1-K186, ref# NM_011982.4)	This paper	N/A
Recombinant protein: Mouse Homer2 EVH1 (aa: M1-D115, ref# NM_011983.2)	This paper	N/A
Recombinant protein: Mouse mGluR1 (aa: P1144-L1199, ref# NM_016976.3)	This paper	N/A
Recombinant protein: Mouse Shank3 (aa: N1284-T1320, ref# NM_021423.3)	This paper	N/A
Recombinant protein: Drebrin HBM1-linker-Homer2 EVH1 (Drebrin L530-E550- GSGENLQGGSGGSGG-Homer2 M1-D115)	This paper	N/A
Critical Commercial Assays		
ViaFect™ Transfection Reagent	Promega	Cat#E4981
Deposited Data		
Crystal structure of Drebrin HBM1/Homer2 EVH1	This paper	5ZZ9
Crystal structure of the Homer1 EVH1/mGluR complex	(Beneken et al., 2000)	1DDV
Solution structure of c-Src SH3 and Class I proline-rich motif	(Feng et al., 1994)	1RPL
Solution structure of c-Src SH3 and Class II proline-rich motif	(Feng et al., 1994)	1PRL
Crystal structure of CIN85 SH3 and ARAP1 proline-rich motif	(Li et al., 2018)	5XHZ
Crystal structure of Dystrophin and Dystroglycan	(Huang et al., 2000)	1EG4
Crystal structure of FE65-WW domain and hMena complex	(Meiyappan et al., 2007)	2HO2
Crystal structure of Mena EVH1 and ACTA complex	(Prehoda et al., 1999)	1EVH
Crystal structure of Profilin and L-Pro10 peptide complex	(Mahoney et al., 1997)	1AWI
Experimental Models: Cell Lines		
Human: COS7 cells	ATCC	CRL-1651; RRID: CVCL_0224
Experimental Models: Organisms/Strains		
Escherichia coli: Rosetta (DE3)	Novagen	Cat#70954
Escherichia coli: BL21 (DE3)	Invitrogen	Cat#C600003
Recombinant DNA		
Plasmid: S142A Drebrin-YFP	Addgene	Cat#58335
Plasmid: pTGFP Human Drebrin	This paper	N/A
Plasmid: pETM.3C Human Drebrin	This paper	N/A
Plasmid: pTRFP Mouse Homer1b	This paper	N/A
Plasmid: pETM.3C Mouse Homer1b	This paper	N/A
Plasmid: pTRFP Mouse Homer1a	This paper	N/A
Plasmid: pETM.3C Mouse Homer1a	This paper	N/A
Plasmid: pETM.3C Mouse Homer2 EVH1	This paper	N/A
Plasmid: pET32M.3C Mouse mGluR1 HBM	This paper	N/A
Plasmid: pET32M.3C Mouse Shank3 HBM	This paper	N/A
Plasmid: pETM.3C Drebrin HBM1-linker-Homer2 EVH1	This paper	N/A

(*Continued on next page*)

Continued

REAGENT or RESOURCE	SOURCE	IDENTIFIER
Software and Algorithms		
Origin7.0 & OriginPro 8.0	OriginLab	http://www.originlab.com/
HKL3000	(Otwinowski and Minor, 1997)	http://www.hkl-xray.com/
PHASER	(McCoy et al., 2007)	http://www.phaser.cimr.cam.ac.uk/
Coot	(Emsley et al., 2010)	http://www2.mrc-lmb.cam.ac.uk/personal/pemsley/coot/
PHENIX	(Adams et al., 2010)	http://www.phenix-online.org/
MolProbity	(Chen et al., 2010)	http://molprobity.biochem.duke.edu/
PyMOL	DeLano Scientific LLC	http://www.pymol.org/
ASTRA6	Wyatt	http://www.wyatt.com/products/software/astra.html
Zeiss blue 2013	Zeiss	https://www.zeiss.com.cn/microscopy/home.html
ImageJ	NIH	https://imagej.nih.gov/ij/
Quantity One	Bio-Rad	http://www.bio-rad.com/

CONTACT FOR REAGENT AND RESOURCE SHARING

Further information and requests for reagents may be directed to, and will be fulfilled by the Lead Contact Mingjie Zhang (mzhang@ust.hk).

EXPERIMENTAL MODEL AND SUBJECT DETAILS

COS7 Cells Culture

COS7 cells derived from the kidney of a male adult African green monkey (from ATCC) were cultured in Dulbecco's Modified Eagle Medium (DMEM) supplemented with 10% fetal bovine serum (FBS) and 50-100 units of penicillin-streptomycin (P/S). Cultured COS7 cells were maintained at 37°C with 5% CO_2. The cell line was not further authenticated. Cells were tested negative for mycoplasma contamination by cytoplasmic DAPI staining.

METHOD DETAILS

Constructs and Protein Purification

The cDNA encoding the human Drebrin fragments (residues 431-649 and 431-548) were PCR amplified using the full-length 70 kDa Drebrin A S142A cDNA template (purchased from Addgene, residues 1-649, NCBI accession code: NM_004395.3). The coding sequences of mouse Homer2 fragment (residues 1-115, NCBI accession code: NM_011983.2), mouse Homer1 full-length (residues 1-354 NCBI accession Number: NM_001284189.2), mouse mGluR1 fragment (residues 1144-1199, NCBI accession code: NM_016976.3) and mouse Shank3 fragment (residues 1284-1320, NCBI accession code: NM_021423.3) were PCR amplified from a mouse cDNA library. All point mutations or deletion constructs were created by PCR-based mutagenesis method. To generate the Drebrin and Homer fusion constructs for crystallization, Drebrin HBM1 (residue 530-550) was fused to the N-terminus of Homer2 EVH1 domain (residue 1-115) by the standard two-step PCR method with a flexible linker 'GSGENLQGGSGGSGG' between the two proteins. All of these constructs were cloned into a modified pET32M.3C vector for protein expression in bacteria or a modified pTGFP/pTRFP vector for expression in COS7 cells.

All proteins were expressed in *Escherichia coli* BL21 (DE3).The N-terminal thioredoxin-His_6-tagged or His_6-tagged proteins were purified with a Ni^{2+}-NTA Sepharose^{TM} 6 Fast Flow column and followed by a Superdex-200 preparation grade size-exclusion chromatography. The purification tag was cleaved by protease 3C and the proteins were further purified by a step of ion-exchange chromatography or another cycle of size-exclusion chromatography.

Fast Protein Liquid Chromatography (FPLC) coupled with static multi-angle light scattering (FPLC-MALS) assay.

Protein samples (typically 180 μL at a concentration of 50-100 μM) were injected into an ÄKTA FPLC system with a Superdex 200 Increase10/300 GL column (GE Healthcare) using the column buffer of 50 mM Tris-HCl pH 7.5, 100 mM NaCl, 1 mM EDTA and 1 mM

DTT. The chromatography system was coupled to a static multi-angle light scattering system equipped with a 18-angle static light scattering detector (Dawn, Wyatt) and a differential refractive index detector (Optilab, Wyatt). The molecular weights were analyzed using the ASTRA 6 software (Wyatt).

Isothermal Titration Calorimetry (ITC) Assay

ITC measurements were carried out on a MicroCal iTC200 (Malvern) at 25°C. All proteins were dissolved in 50 mM Tris-HCl (pH 7.5) buffer containing 100 mM NaCl, 1 mM EDTA and 1 mM DTT. The concentrations of the protein in the syringe were typically 500 μM, while the concentrations of the protein in the cell were typically 50 μM. Each titration point was performed by injecting a 2 μL aliquot of the syringe sample into the cell sample at a time interval of 120-150 s to ensure that the titration curve returned to the baseline. The titration data were analyzed by Origin7.0 and fitted by the one-site binding model.

Crystallography

Crystals of the Drebrin and Homer2 fusion complex (protein in 50 mM Tris-HCl pH 7.5, 100 mM NaCl, 1mM EDTA and 1 mM DTT) were obtained by the sitting drop vapor diffusion method at 16°C. The crystals were initially grown in buffer containing 50 mM ammonium fluoride and 8% w/v polyethylene glycol 3,350, and further optimized in the above buffer with additional 0.20% w/v adenosine 5'-triphosphate disodium salt hydrate, 0.20% w/v 2'-deoxycytidine 5'-monophosphate sodium salt, 0.20% w/v β-estradiol, 0.20% w/v D-(+)-galactose, 0.20% w/v 2'-deoxyguanosine hydrate, and 0.02 M HEPES sodium pH 6.8 (Silver bullet bio additive). The crystals were soaked in crystallization solution containing additional 10% v/v glycerol for cryo-protection. Diffraction data were collected at the Shanghai Synchrotron Radiation Facility BL19U1 at 100 K. Data were processed and scaled using HKL3000 (Otwinowski and Minor, 1997). Structure of the Drebrin HBM1/Homer2EVH1 complex was solved by the molecular replacement with the Homer1 EVH1 structure as the search model (PDB code: 1DDV) using PHASER (McCoy et al., 2007). Further manual model building and refinement were completed iteratively using Coot (Emsley et al., 2010) and PHENIX (Adams et al., 2010). The final model was validated by MolProbity (Chen et al., 2010). The final refinement statistics are summarized in Table 1. All structure figures were prepared by PyMOL (http://www.pymol.org).

Actin Bundling Assay

Rabbit skeletal muscle actin (Cytoskeleton) were dissolved in ddH_2O and hydrated in 5 mM Tris-HCl in pH 8.0 and 0.2 mM $CaCl_2$ supplemented with 0.2 mM ATP and 0.5 mM DTT on ice for 1h and centrifuged at 150,000-200,000 g for 20 min at 4°C. Actin concentration in the supernatant was determined by absorbance at 290 nm using the Lambert-Beer law. Actin was polymerized at room temperature for 1h after adding one-tenth volume of 10× polymerization buffer (500 mM KCl, 20 mM $MgCl_2$ and 10 mM ATP). Bundles were prepared by mixing 4 μM F-actin with 1 μM Drebrin FL WT/S142E and incubating at room temperature for 1h, with or without 1 μM of various forms of Homer1 in the mixtures. For co-sedimentation assay, mixtures were centrifuged at 4°C 10,000g for 20min. After centrifugation, supernatants (solutions) were transferred to new tubes. Pellets (F-actin bundles) were washed once by the same assay buffer and centrifuged again at 4°C 10,000g. For fluorescence microscopy, F-actin was labeled with Alexa Fluor 555 Phalloidin (AF555-Phalloidin). Aliquots (5-10 μL) were delivered onto microscope slides. A coverslip was then placed over each drop of the samples gently. All the samples were imaged using a Zeiss LSM 710 laser-scanning confocal microscope, and images were processed with Zeiss blue 2013. The relative fluorescence intensity was defined as: Total fluorescence intensity/Area of bundled F-actin. Samples for TEM were adsorbed to glow-discharged, carbon-coated formvar films on copper grids for 1 min and negatively stained with 1% (m/v) uranium acetate (UA) for 30 s. EM images were acquired using a HITACHI TEM-HT7700 transmission electron microscope and processed with ImageJ. For the Homer1a competition assay, increasing concentrations of Homer1a were mixed with F-actin-Drebrin-Homer1b (4:1:1) and the mixtures were incubated for 1h. F-actin bundles were assayed by co-sedimentation and FM imaging methods. All groups were compared with the Drebrin FL S142E + Homer1b FL WT group by the two-tailed independent sample T test in the IBM SPSS Statistics 19 software.

Actin Binding Assays

For actin binding experiments, samples were centrifuged at 250,000g for 25 min, at 4°C, in a Beckman TLA-100 rotor. After centrifugation, pellets were solubilized in 1× gel sample buffer and analyzed by SDS-PAGE. To quantify the amount of Drebrin co-sedimented with F-actin in pellets, we loaded 0.1-8 μM of purified Drebrin as the standards. Binding parameters (K_d and Bmax) are obtained by fitting the average data points with Hill model in OriginPro 8.0.

Cell Imaging and Data Analysis

Before transfections, $3\sim4\times10^4$ cells were plated on 12-well cell culture plates and allowed to adhere overnight. At12-16 h later, cells were transiently transfected using ViaFect™ Transfection Reagent (Promega) following the manufacturer's instruction. At 8-10 h post-transfection, cells were plated on acid washed 18-22 mm square 1.5-1.8# glass coverslips. Images were taken at 12-16 h after cell adhesion on the coverslips. These cells were not individually authenticated and not found to be on the list of commonly misidentified cell lines (International Cell Line Authentication Committee). Cells were tested negative for mycoplasma contamination by cytoplasmic DAPI staining. All the images were acquired on a Zeiss LSM 710 laser-scanning confocal microscope, with a 40×1 or 63×2 oil objective and pinhole setting to 1 Airy unit. Data were collected from three independent batches of cultures. In each group, at least 60 fluorescence-positive cells were counted for each group of experiments. All experiments were conducted in a double-blinded

fashion. The length and number of primary filopodia (crossing the cell edge with length > 2μm) in each cell were quantified by Zeiss blue 2013 and analyzed using OriginPro 8.0.

QUANTIFICATION AND STATISTICAL ANALYSIS

Data of *in vitro* Actin bundling sedimentation assay and COS7 cell filopodial number were expressed as mean ± SD. Data of FM/TEM imaging and COS7 cell filopodial length were expressed as boxplot. The statistical analysis was performed using two-tailed independent sample T test in the IBM SPSS Statistics 19 software; n.s, not significant, *$p<0.05$, **$p<0.01$, ***$p<0.001$. All experiments related to FM/TEM imaging, cell cultures and COS7 imaging studies were performed in blinded fashion.

DATA AND SOFTWARE AVAILABILITY

Data Resources

The atomic coordinates of Drebrin HBM1/Homer2 EVH1 complex have been deposited to the Protein Data Bank under accession code PDB: 5ZZ9.